

Cluster Dynamics in a Circulating Fluidized Bed

Chris Guenther and Ronald Breault

*US Department of Energy, National Energy Technology Laboratory
Morgantown, WV 26507, USA*

Abstract

A common hydrodynamic feature in industrial scale circulating fluidized beds is the presence of clusters. The continuous formation and destruction of clusters strongly influences particle hold-up, pressure drop, heat transfer at the wall, and mixing. In this paper fiber optic data is analyzed using discrete wavelet analysis to characterize the dynamic behavior of clusters. Five radial positions at three different axial locations under five different operating were analyzed using discrete wavelets. Results are summarized with respect to cluster size and frequency.

1. Introduction

Circulating fluidized bed technology (CFB) is being used in a variety of metallurgical, chemical and energy processes. In the energy sector, one of the promising applications of CFB's is the use of transport gasifiers in advanced coal-fueled power systems. Power plants of the future e.g., Clean Coal Power Initiative (CCPI) and FutureGen power plants will both use CFB technology. Transport gasifiers because of their ability to operate at high throughput conditions, achieve better mixing i.e., increase mass and heat transfer, and achieve higher carbon conversion will be a key component in the overall plant design. Given such an important role these gasifiers will have on energy plants of the future and the influence clusters have on overall CFB operation, a comprehensive characterization of cluster dynamics is critical for their design, scale-up, and operation.

The multi-resolution capability of wavelets and their well known excellence in time frequency localization makes wavelets an ideal tool to investigate cluster dynamics. Under certain operating conditions cluster length can vary by an order of magnitude which requires the multi-resolution capability of wavelets. This investigation uses wavelets to analyze fiber optic data taken in the riser section of the cold flow circulating fluidized bed facility at National Energy Technology Laboratory (NETL). Results are presented which quantify the cluster size and frequency at five radial positions and three different axial locations as reported in [1]. Three different superficial gas velocities and three different mass circulation rates are investigated. The different flow conditions investigated span the fast fluidization, dilute up flow, and core-annular regimes. The fiber optic data used in this investigation was previously used to determine time average solids velocities [2] at radial and axial positions indicated in this paper. The solid velocities are used in the determination of cluster length and a discussion is presented in Section 3.3. The effect of local solids velocities is also presented in this paper and results are compared to results reported in [1].

Table 1 Cork Properties.

Symbol	Units	Value
ρ_s (particle density)	kg/m ³	189
ρ_b (bulk density)	kg/m ³	95
d_p (particle diameter)	μm	812
U_t (terminal velocity)	m/s	.86
U_{mf} (minimum fluidization velocity)	m/s	.07
ε (void fraction)		.49
ϕ (sphericity)		.84

The fiber optic probe used in this investigation was from Vector Scientific Instruments. The probe consisted of two fiber bundles vertically stacked a known optical distance apart. Each bundle contains both light producing and light receiving fibers. As particles travel past the bundle the reflected light (voltage) is calculated by the different light producing and light receiving fibers within a bundle. An average voltage is generated for each bundle. By shifting one voltage signal and holding the other constant, and visa versa, a curve can be constructed that is a function of the time shift and a correlation coefficient. By determining the maximum peak in the correlation curve, the solids velocity can be calculated using that time shift and the known optical distance between the two fiber bundles. This procedure was repeated 200 times, data was collected at a frequency of 12.5 kHz which generates 4096 samples for each of the 200 time series. This result is a 65.5 second time series of 819,200 data points. For each repeat of 200 times a correlation curve was generated and a corresponding solids velocity. The 200 solids velocities were then averaged generating an average solids velocity for each radial and axial position for the entire test matrix. By shifting the voltage signal both ways with respect to the two bundles during the correlation step to determine if the curves correlate better at the beginning or terminal part of the curve results in the knowledge of which bundle lags the other. Knowing the lag allowed up solid velocities to be distinguished from down solids velocities which is critical in a core-annular flow regime.

Figure 3 shows the range of operating conditions that were run for the cork material. For each condition fiber optic data was collected at three different axial locations and five different radial positions referred to in this paper as P0, P1, P2, P3, and P4. These radial points are a distance of .12, .07, .05, .03, and .01 meters from the wall respectively and were selected to give equal annular areas. Table 2 lists the different operating conditions from the test matrix used in this investigation and Table 3 summarizes the axial solids velocities [2] for each of the radial positions and operating conditions considered in this investigation.

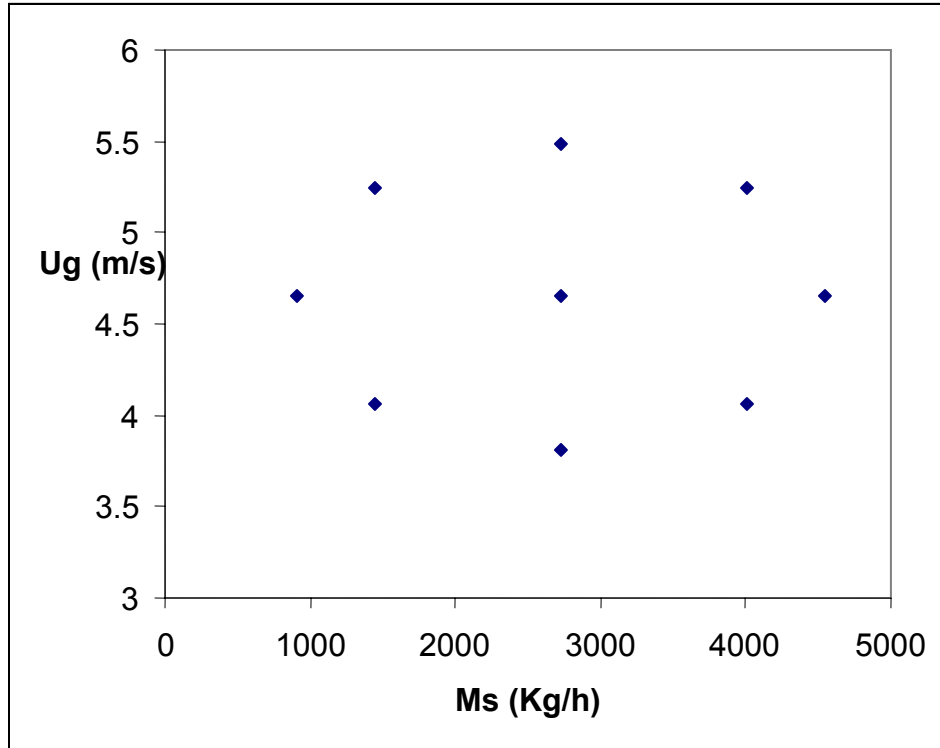


Figure 3 Experimental test matrix.

Table 2 Operating conditions used in this paper.

Ug (m/s)	Ms (Kg/h)
3.81	2727
4.65	909
4.65	2727
4.65	4545
5.49	2727

Table 3 Solids axial velocities.

Axial Velocities (m/s)					
Elevation 3.9 m	3.81 m/s 2727 Kg/h	4.65 m/s 909 Kg/h	4.65 m/s 2727 Kg/h	4.65 m/s 4545 Kg/h	5.49 m/s 2727 Kg/h
P0	6.16	4.64	6.82	7.53	7.37
P1	4.53	3.93	4.69	4.87	5.54
P2	3.79	3.09	3.11	3.78	4.12
P3	2.26	2.39	0.94	2.62	1.08
P4	-0.50	0.05	-0.94	1.38	-0.51
Elevation 8.3 m					
P0	7.01	4.97	7.94	8.62	7.87
P1	5.06	4.49	6.33	6.24	6.76
P2	3.54	4.01	4.57	4.33	5.42
P3	2.06	3.69	2.69	2.36	3.78
P4	-0.64	3.25	-1.19	-0.97	-0.56
Elevation 12.1 m					
P0	7.47	4.86	8.36	9.00	9.56
P1	5.06	4.44	5.97	6.03	7.50
P2	3.61	3.99	4.57	4.34	5.16
P3	2.10	3.28	2.57	2.85	3.08
P4	-0.34	2.77	-0.78	-0.30	-0.15

3. Data analysis

3.1 Analysis of cluster data

A typical output signal from one of the fiber bundles is shown in the Figure 2. The signal represents the light intensity that is reflected off of the particles in the riser. High signal levels imply many particles close to the probe tip and no signal (zero value) represents zero particles. The distribution of this data is not normally distributed. The significance of this fact is that the mean and standard deviation have no meaning and therefore, the identification of phenomena based upon the mean and standard deviation has no meaning. Hence, the fiftieth percentile was used in the cluster analysis presented in this paper.

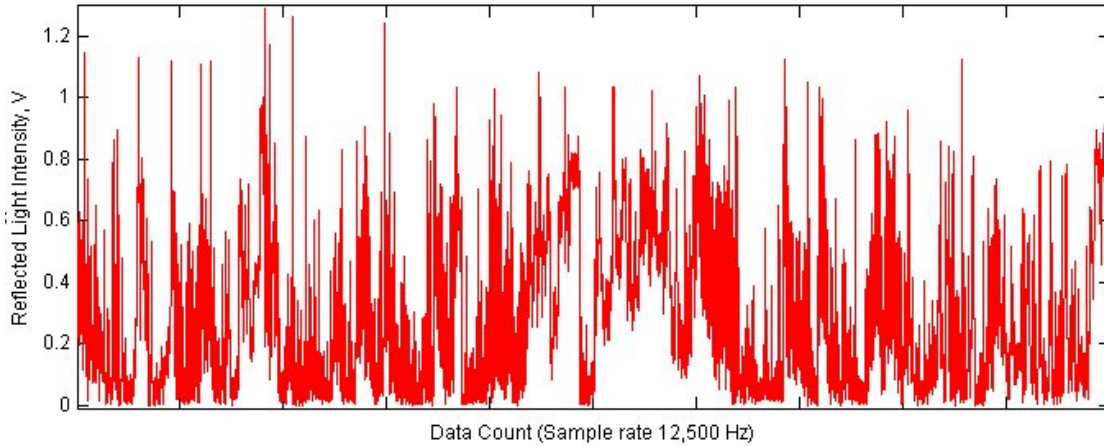


Figure 2 Reflected light intensity over time.

3.2 Wavelet analysis

The wavelet transform of a given signal $f(t)$ can be defined as

$$W_s f(t) = \int_{-\infty}^{\infty} f(u) \psi_s(t-u) du . \quad (1)$$

For most practical applications the continuous dilation and translation given in Equation (1) is replaced with a discrete representation. That is, the dilation is represented by $s = 2^j$ and translation or shift is $t = k/2^j$, k a constant. Then a series of discrete wavelet filters are generated each one representing a different frequency band or level of detail of the original time series $f(t)$.

Wavelets have been used successfully in other investigations to investigate pressure fluctuations in a bubbling bed [4] and clusters in a downer [5]. In both of these investigations wavelets were used to resolve data containing large and small length and time scales into corresponding low and high frequency components. The high frequency components were used to identify bubbles in the pressure fluctuation signal and clusters from the micro-video data. In both of these investigations flow conditions produced very clear spikes in the time series which represented the passing of a bubble or cluster. Under these conditions spikes in the time series can be easily detected by identifying inflection points or local extrema in the high frequency component. Because the time series considered in this paper were so chaotic and clusters were occurring on very small length and time scales, the high frequency component could not be used with confidence to identify clusters. Fiber optic data taken at NETL showed spiking throughout the time series, very near clusters and within the cluster itself which can be seen in Figure 4. The wavelet analysis in this investigation showed that sudden changes in the detail coefficients (high frequency component) do correspond to changes in the voltage signal. However, the difficulties were which level of detail coefficient to use to identify a cluster and for any given level similar spikes in the voltage signal produced very different representations in the detail coefficients making it very difficult to identify and compare clusters. Furthermore,

for clusters traveling at an angle to the probe, which was more the norm than the exception, none of the detail levels adequately represented how long the cluster existed in the time series. Because of these problems it was decided to reconstruct the signal using both the high and low frequency components of the decomposition to identify clusters. It is well-known that any time series can be reconstructed from a wavelet decomposition by taking a particular approximation level and adding the corresponding detail level plus the remaining high frequency detail coefficients.

In this investigation Matlab's ® wavelet toolbox was used for the analysis of clusters. The use of the discrete wavelet in this investigation had two primary roles. The first was to obtain an appropriate wavelet and a corresponding scale or approximation level to accurately resolve clusters as small as six particle diameters, which for this investigation would be clusters approximately .005 m in length. Clusters of length six particle diameters (.005 m) were identified in Breault et al. [6] as the smallest detectable cluster for cork material using laser Doppler velocimetry (LDV). The Daubechies Wavelet [7] of order three (DB3) was chosen for all the analysis reported in this paper. This wavelet was chosen because for a given order and scale it resulted in smaller residuals than other wavelets tested. For the smallest length scales in this investigation the DB3 scale three approximation accurately resolved the smallest clusters of interest. The second role was to ensure that the wavelet scale chosen functioned as an appropriate low pass filter. In the vicinity of the wall, the dominate cluster velocity is about 1m/s [8] and [9] also confirmed by Zinn [2]. The fiber optic bundle used at NETL was 1 mm in diameter denoted in Figure 3 by (d) while the length of a cluster is given by (L). For a cluster passing the probe tip at a velocity of V_c , the time Δt is given by $(L+d)/V_c$. For a cluster of length .008 m traveling downward at the wall at 1 m/s, Δt would be .009 s. This corresponds to a frequency of approximately 111 Hz and if the same cluster was moving up in the center of the riser where axial solids velocities can reach 8.5 m/s, Δt would be .001 s corresponding to a frequencies of 944 Hz. Under these types of conditions and applying Nyquist's limit, one can determine the minimum frequency needed to retain to accurately resolve the signal and thereby determine which detail coefficients can be excluded in the reconstruction of the signal. To remove high frequency noise from the reconstruction the contributions from the first two detail coefficients were not used and the approximation chosen to reconstruct the signal was level three retaining on the level three detail coefficients. Choosing DB3 scale three approximation and retaining only the level three detail coefficients to reconstruct the signal effectively removed high frequencies noise above the Nyquist limit of 1888 Hz for small clusters at the center of the riser. The high frequency noise was mainly due to the probe using a modulated light source to improve the signal to noise ratio and minimize the effect of background light.

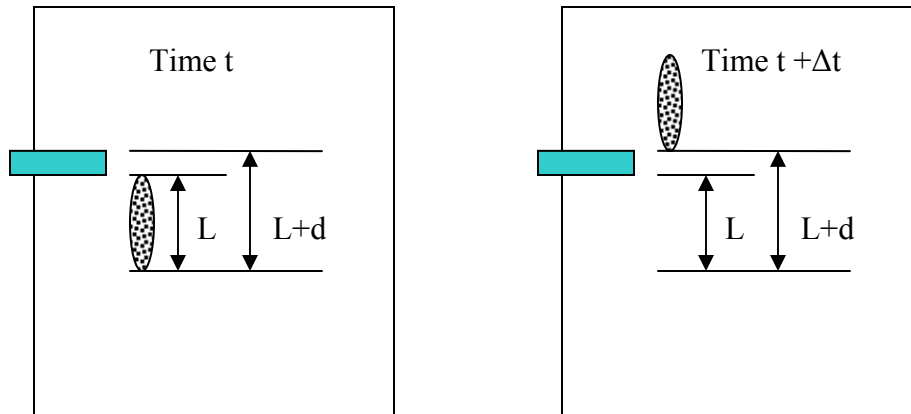


Figure 3 Time scales of a typical cluster configuration.

3.3 Cluster size determination

The algorithm to identify clusters and their respective sizes is quite simple and straight forward. First, for a given flow condition and spatial position the value of the 50th percentile is determined. Next, the value of the reflected light intensity in volts is compared to the 50th percentile value. A vector containing a series of 0s and 1s is constructed, if the value is less than the 50th percentile, the data is identified with a 0 and if the data is greater than or equal to the 50th percentile, it is identified with a 1. The length of the cluster in terms of number of consecutive data points is obtained by summing the consecutive 1s in the above noted vector. This value is then multiplied by the time averaged solids velocity listed in Table 3 to give the length of the cluster in meters. Since only macro-clusters are being considered in this analysis, cluster lengths less than 20 data points are discarded as being micro-clusters. The lengths of the clusters are binned in 0.005 m bins to produce a histogram. The average cluster size is then computed by summing the product of the bin size and the cluster count in the respective bin for all bin sizes and then dividing this quantity by the total cluster count. This analysis is done for each radial position and riser height for each of the five gas velocity - solids flow rate pairs being discussed.

4. Results and discussion

4.1 Increased solids circulation rate

Figure 4 shows the cluster count and size at three elevations for a fixed superficial gas velocity of 4.6 m/s and three different solids circulation rates 909, 2727, and 4545 Kg/h. For these solids circulation rates the flow regime changes from dilute up flow (909 Kg/h) to core annular for both the 2727 and 4545 Kg/h cases. Clearly, the cluster size increased at each elevation and every radial position as the solids loading increased. These results show that cluster size dramatically increased from the dilute up flow regime to the core annular regime for two highest elevations 12.1 m and 8.3 m and a smaller increase was found at the lowest elevation of 3.9 m. Cluster size was the largest near the wall at the

highest elevation. However, the cluster size was more uniformly distributed at 8.3 m elevation and at the 3.9 m elevation the largest clusters were found towards the center of the riser. In Figure 5 the cluster size was averaged across each radial position. Again size increased as loading increased with the most dramatic changes in size taking place when the flow regime changed from dilute up flow to a core annular regime. Figure 4 shows that in general as the solids circulation rate increased cluster count decreased towards the wall and generally increased towards the center of the riser. However, Figure 5 shows that the average cluster count at each elevation remained fairly constant for each solids circulation rate even as one moves from the dilute to the core annular regime.

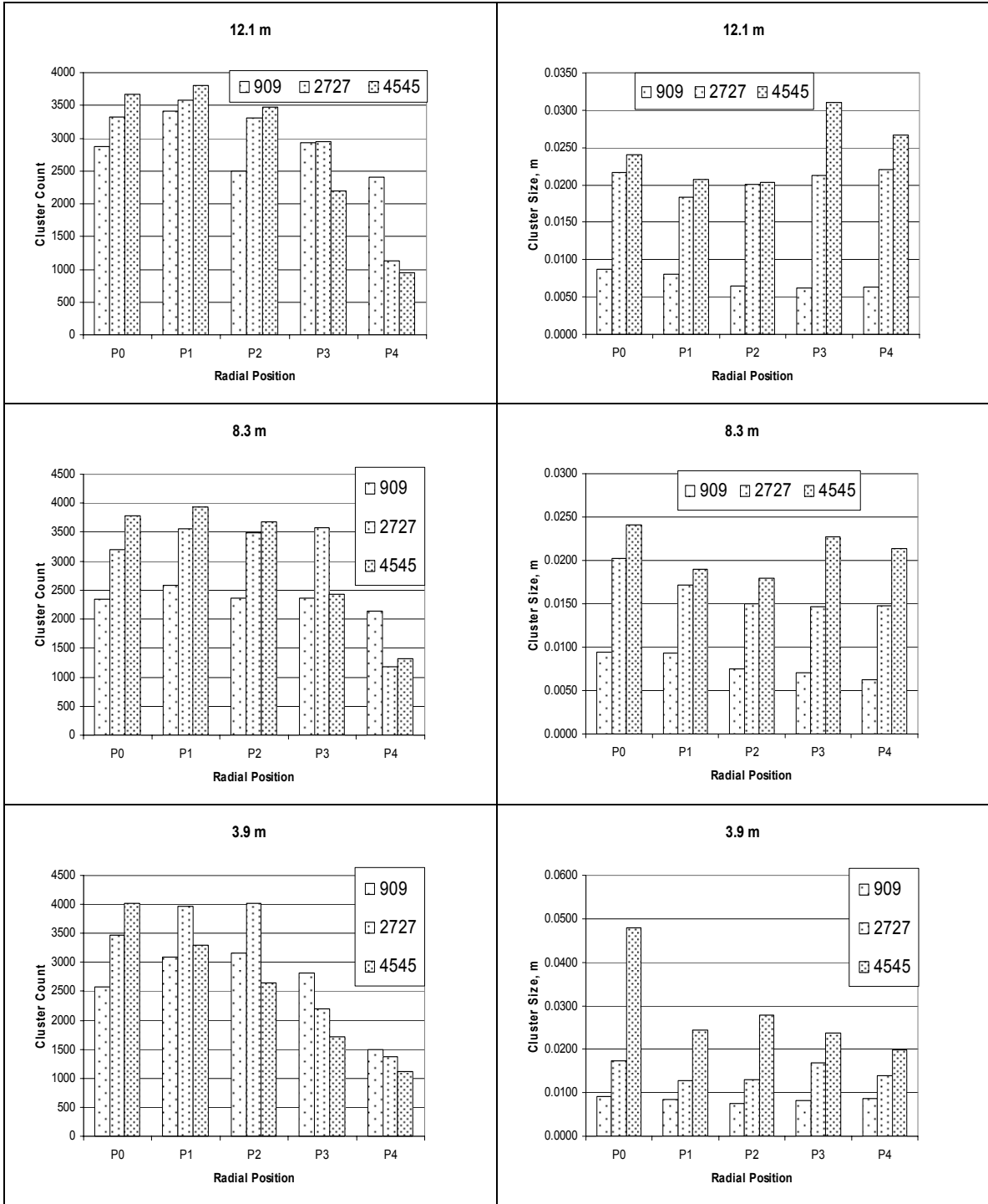


Figure 4 Axial cluster count and size for a fixed gas velocity of 4.6 m/s and mass circulation rates of 909, 2727, and 4545 Kg/h [1].

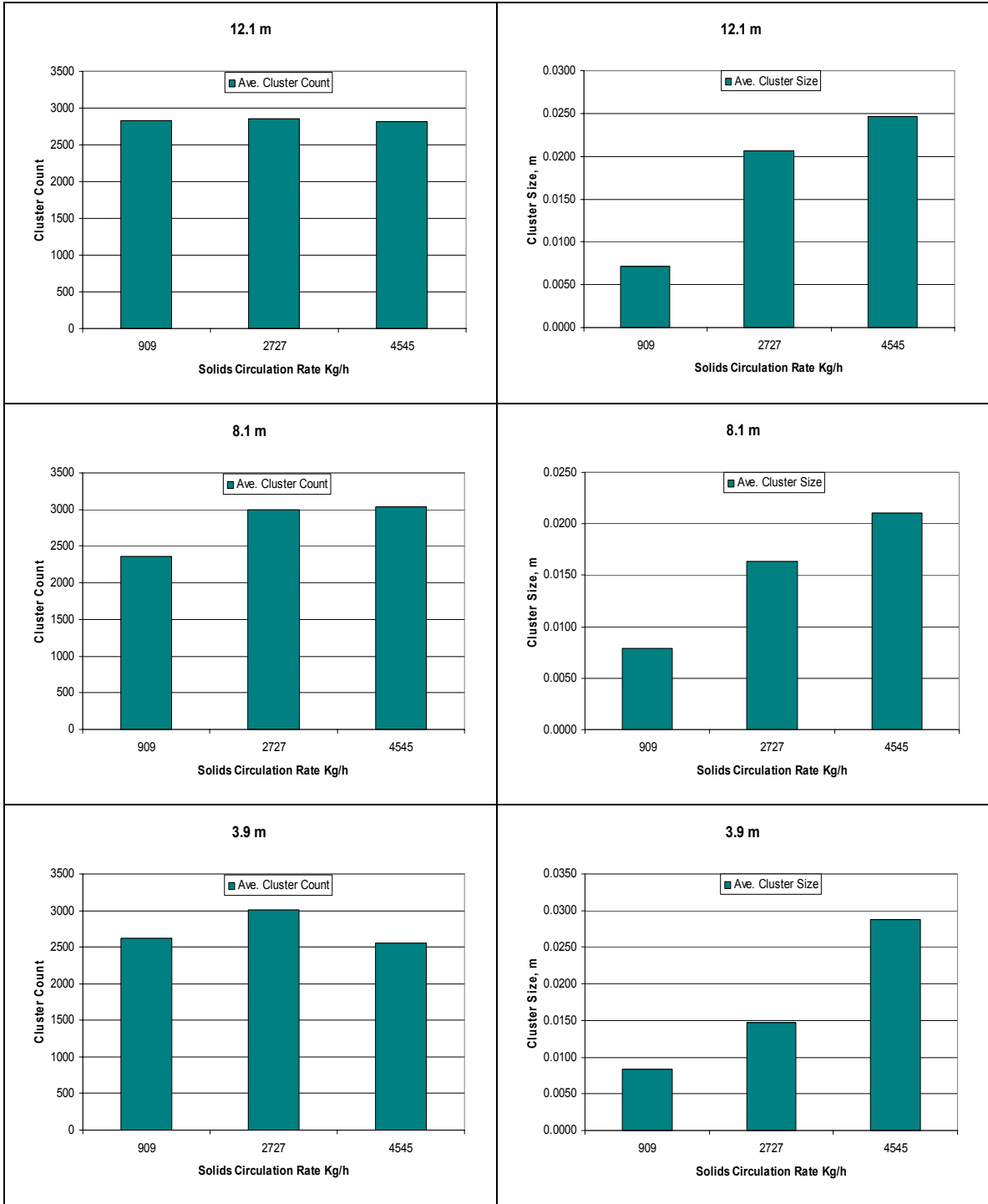


Figure 5 Spatially averaged cluster count and size across each radial position for a fixed gas velocity of 4.6 m/s and mass circulation rates of 909, 2727, and 4545 Kg/h [1].

4.2 Increased gas flow rate

Figure 6 shows the cluster count and size for a fixed solids circulation rate of 2727 Kg/h and three different gas velocities 3.8, 4.6, and 5.2 m/s. Cluster size remained fairly uniform across the radius at the highest elevation for each gas velocity. At the 8.3 m and 3.9 m elevations very little change in cluster size was observed for the 4.6 m/s and 5.2 m/s cases, which for these velocities are both in the core annular flow regime. The largest changes occurred at the two lower elevations as the gas velocity increased above 3.8 m/s taking one from the fast fluid bed regime to the core annular regime. However, comparing these results to section 4.1 shows that cluster size is much less sensitive to changes in the gas velocity compared to changes in the solids circulation rates. Figure 7 shows cluster count and size spatially averaged across each radial position for a fixed solids circulation rate. Clearly, very little change in cluster size and cluster count at all the elevations is observed at the two highest velocities both of which are in the core annular flow regime. The largest changes in cluster size occurred at the lower elevations as conditions changed from fast fluid bed (3.8 m/s) to core annular (4.6 m/s). The only significant change in average cluster count was at the lowest elevation as the velocity increased from 3.8 m/s to 4.6 m/s.

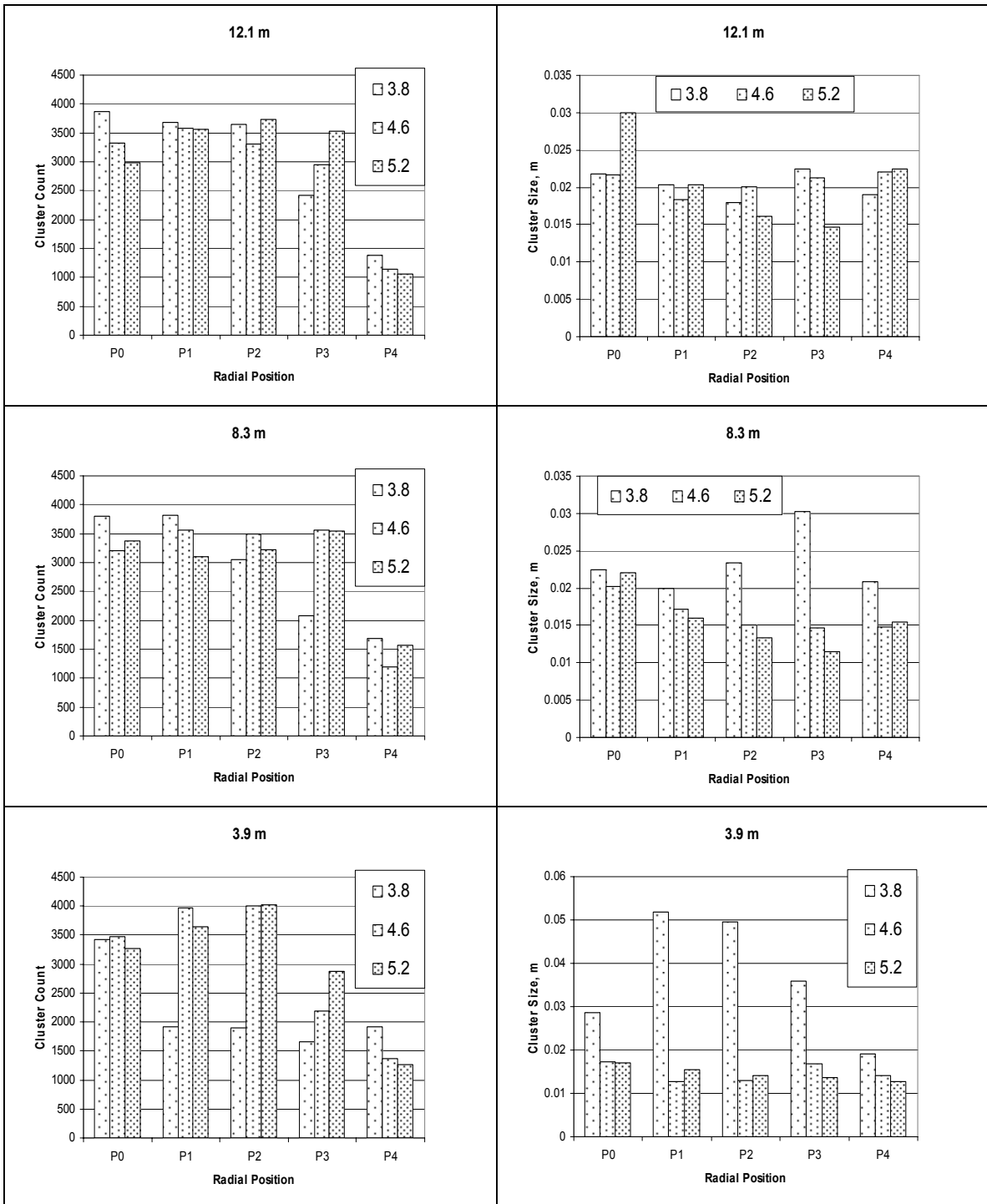


Figure 6 Axial cluster count and size for a fixed mass circulation rate of 2727 Kg/h and gas velocities of 3.8, 4.6, and 5.2 m/s [1].

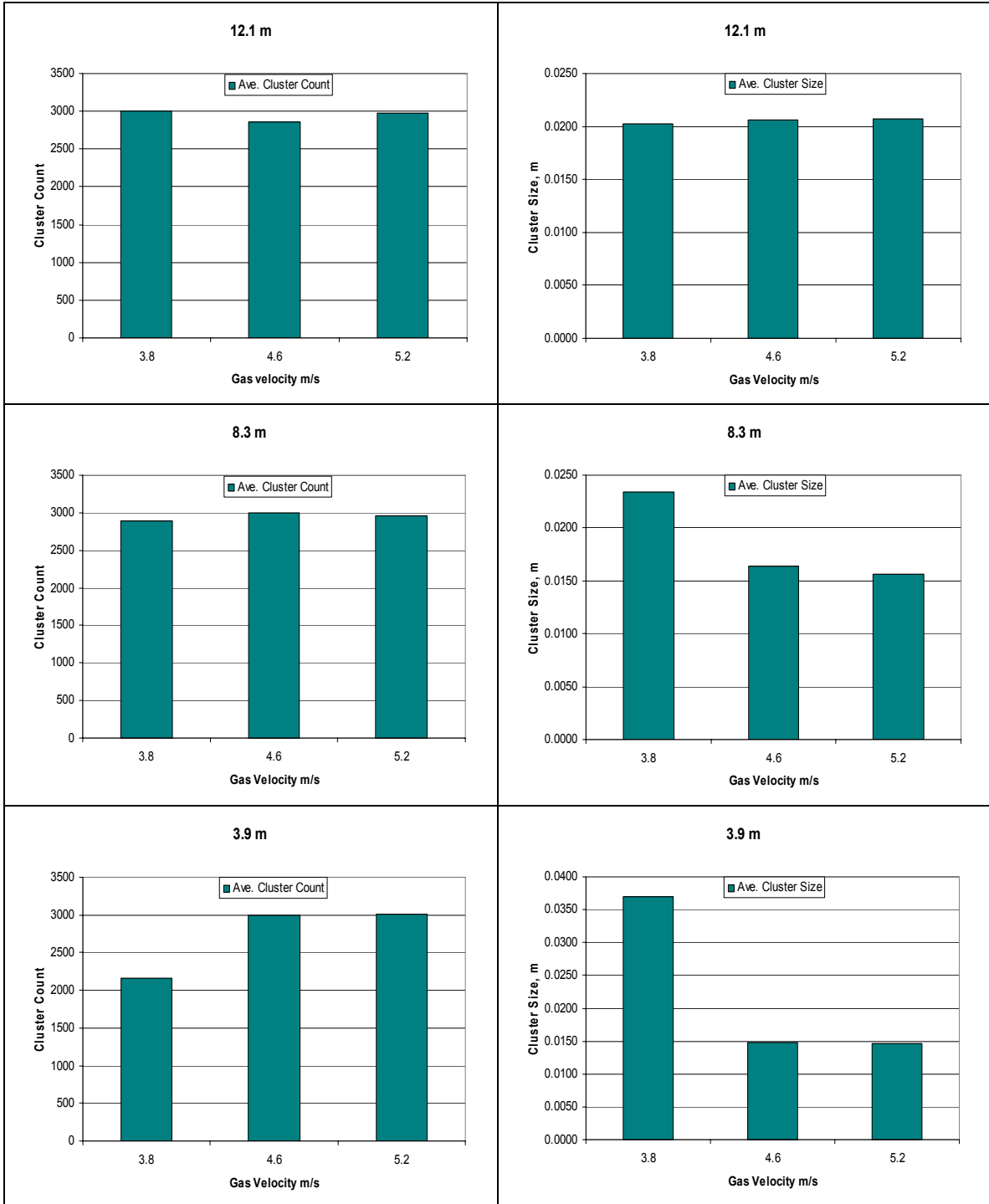


Figure 7 Spatially averaged cluster count and size across each radial position for a fixed solids circulation rate of 2727 kg/h and gas velocities of 3.8, 4.6, and 5.2 m/s [1].

4.3 Further analysis of cluster dynamics

One of the unexpected results of this investigation was the cluster count towards the center of the riser compared to the cluster count towards the wall. Both Figure 4 and Figure 6 show a larger number of clusters towards the center of the riser compared to the cluster count at the wall for all elevation and all flow conditions. Also, these figures show that in general cluster size is greater at radial positions away from the wall compared to the location (P4) nearest the wall. These findings are somewhat counter intuitive especially when operating in the core annular regime. The fact that near the wall location (P4) is unable to maintain large cluster sizes can be attributed to the complex hydrodynamics that are inherent in this region especially core annular flow regimes. Wall effects and if operating in the core annular regime high solids loading near the wall tend to break up clusters producing micro-scale clusters (less than six particle diameters). Where locations away from the wall are more homogeneous and are able to sustain larger clusters. In general this investigation found that cluster size distributions shifted towards a smaller cluster size near the wall and at P4 cluster count dropped significantly due to cluster size falling below the minimum size considered in this investigation of 0.005 m.

Finally, this investigation also analyzed the fiber optic data as described in section 2 using significantly smaller number of data points to correlate. The goal was to investigate the effect local solids velocities had on the cluster results compared to a single solids velocity given by the 65.5 time average reported in Table 3. The data was analyzed correlating 256 samples rather than 4096. Correlation curves were generated by shifting in both directions a total of 128 data points resulting in a solids velocity every 0.02 seconds. These velocities were then used in the determination of the cluster size discussed in section 3.3. Results showed that the general trends shown in figures 4-7 did not change. That is, cluster count remained larger away from the wall and cluster size remained smaller towards the wall. However, the analysis did show that the local velocities did produce a smoother transition in the cluster count across the radial positions. Figure 8 shows the count at P4 increased and decreased at P1-P3 resulting in a monotonically decreasing count across the radius. Local velocities had less of an effect on the cluster size which can be seen in Figure 9.

8.3 m

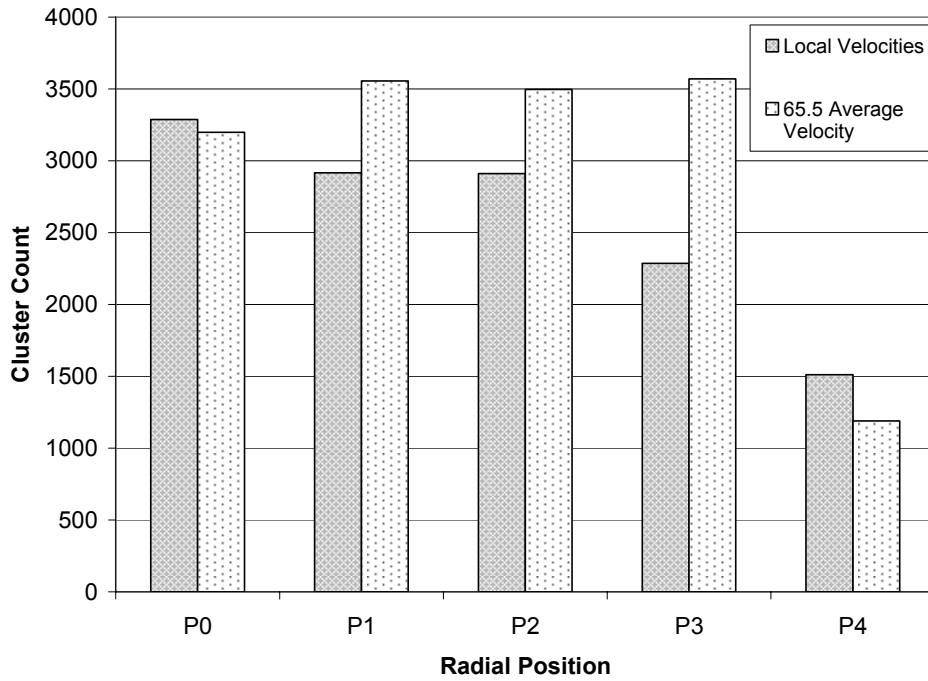


Figure 8 Cluster count comparison of the solids velocities calculated every 0.02 s with velocities reported in Table 3 for the case of 2727 kg/h and 4.6 m/s.

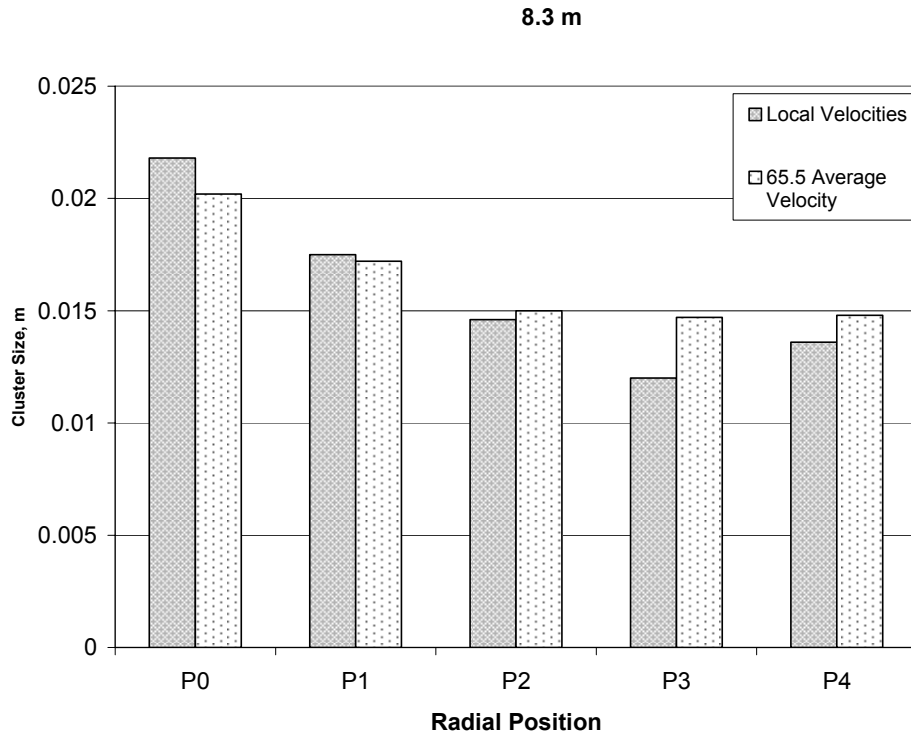


Figure 9 Cluster size comparison of the solids velocities calculated every 0.02 s with velocities reported in Table 3 for the case of 2727 kg/h and 4.6 m/s.

6. Summary

This paper investigated cluster size and count at a variety of radial and axial positions in a large scale circulating fluidized bed under three different flow regimes. The results showed the most dramatic changes in the cluster size and count occurred when flow conditions changed from one regime to another. The results showed an increase in the solids circulation rate at a fixed gas velocity had more impact on the cluster dynamics than changes in gas velocity for a fixed solids circulation rate. Results showed that for the cluster sizes tracked in this investigation cluster count generally decreased towards the wall and increased towards the center of the riser. Spatially averaged results shown in Figure 5 and Figure 7 show that when operating in a core annular regime changes in gas velocity do not impact the cluster size, but changes in the solids circulation rate does. These figures also show that when operating in the core annular regime average cluster count for a given axial location remains fairly constant with respect to changes in the gas velocity or solids circulation rates. The results showed that locations away from the wall were able to maintain larger cluster sizes than the location nearest the wall. Finally, local solids velocities showed very little effect on the cluster dynamics and general trends reported in this investigation.

7. Acknowledgements

The authors would like to thank Anthony Zinn of REM Engineering Services, PLLC of Morgantown, WV, 26505 for installing the VSI probe, collecting data, and generating solids velocity data for the experimental matrix considered in this investigation.

8. References

- [1] C Guenther and R. Breault, Wavelet analysis to characterize cluster dynamics in a circulating fluidized bed, submitted to Powder Technol.
- [2] A. Zinn, E. Monazam, J. Spenik and J. Ludlow, REM laser probe contract results and summary, DOE/NETL-2006/1229 (2006).
- [3] E. Ghordzoe, P. Smith, P. Vimalchand, G. Lui and J. Longanbach, Initial operations of the PSDF transport gasifier, *Proceedings of the 16th International Conference on Fluidized Bed Combustion*, FBC01-0065, Reno, Nevada, USA (2001).
- [3] X. Lu and H. Li, Wavelet analysis of pressure fluctuation signals in a bubbling fluidized bed, *Chem. Eng. Sci.*, **75** (1999), pp. 113-119.
- [5] X. Lu, S. Li, L. Du, J. Yao, W. Lin and H. Li, Flow structures in the downer circulating fluidized bed, *Chem. Eng. J.* **112** (2005), pp. 23-31.
- [6] R. Breault, J. Ludlow and P. Yue, Cluster particle number and granular temperature for cork particles at the wall in the riser of a CFB, *Powder Technol.* **149** (2005), pp. 68-77.
- [7] I. Daubechies, Ten lectures on wavelets, *Soc. for Ind. and Applied Mathematics*, Philadelphia, PA, USA (1992).
- [8] P. Noymer and L. Glicksman, Descent velocities of particle clusters at the wall of a circulating fluidized bed, *Chem. Eng. Sci.*, **55** (2000), pp. 5283-5289.
- [9] D. Gidaspow, Y. Tsuo and K. Luo, Computed and experimental cluster formation and velocity profiles in circulating fluidized beds, *Fluidization IV*, Banff, Alberta, Canada (1989).